Role of Sigma Phase on Hydrogen Embrittlement of Super Duplex Stainless Steels †

KURODA Toshio*

Abstract

The role of sigma phase on corrosion and hydrogen embrittlement of super duplex stainless steels was investigated by using corrosion tests, transmission electron microscopy (TEM) and fractography. The materials used were type 329J1, SAF2205 and SAF2507 duplex stainless steels. The specimens were heated at 923K to 1223K in order to investigate the precipitation of sigma phase (Fe-Cr-Mo compound).

The evaluation of corrosion was made using a 10% oxalic acid test (ASTM A262A) and Strauss test (ASTM A262E). Hydrogenation of the specimens was achieved by cathodic charging in a 5%H_2SO_4 solution and the hydrogen embrittlement was evaluated using slow strain rate testing (SSRT). The duplex stainless steels consist of ferrite and austenite microstructure. The secondary austenite was preferentially corroded but the sigma phase was hardly corroded by using ASTM A-262A and A262E tests. The sigma phase enhanced hydrogen embrittlement. The fracture morphology showed that the fracture facet size was related to the sigma phase precipitated around austenite. The crack due to hydrogen embrittlement occurred and propagated at the sigma-ferrite interface on the basis of the 3-D reconstruction system of fractography.

KEY WORDS: (Duplex stainless steel),(Hydrogen Embrittlement),(Corrosion), (Microstructure), (Sigma phase), (Secondary austenite), (Fractography)

1. Introduction

Duplex stainless steels are suitable for many marine and petrochemical applications, particularly where chlorides are present because of their attractive combination of mechanical and corrosion properties [1, 2].

Duplex stainless steels having two-phase ferrite-austenitic microstructure include a wide range of alloys ranging from low-alloy grades to the high-alloy duplex grades such as type329J1.

High-alloy super duplex stainless steels have been developed to current requirements for pitting and stress corrosion cracking in chloride environments. These steels contain sufficient amounts of chromium, molybdenum, and nitrogen such as SAF2205.

Super duplex stainless grade such as SAF2507 is a high alloyed duplex stainless steel of type 25%Cr-7%Ni -3.2%Mo-0.27%N having Pitting Resistance Equivalent (PRE) values above 40. But, in the temperature range 573K-1323K, sigma (σ) phase can be observed [3)-8)]. Although many phases are formed, sigma phase is by far the most important because of its large volume fraction, and its influence on toughness and corrosion behavior is biggest.

Sigma phase having a tetragonal structure is basically Fe-Cr-Mo intermetallic compound (According to ASTM Card 5-0708 lattice parameter, a=0.879nm, c=0.447nm) [3),4)]. SAF2507 having a higher level PRE value has a chemical composition of 25%Cr-7%Ni- 3.2%Mo, in which precipitation of sigma phase is therefore expected to occur more rapidly. Precipitation of sigma phase is well known to causes the lowering of the toughness[7)-13)].

It was reported that duplex stainless steel containing ferrite is subject to hydrogen embrittlement while fisheyes were observed and welding cracks associated with hydrogen occurs more than 7ppm in Ferralium259 duplex stainless weld metal [14)].

In this investigation, the role of σ phase on corrosion and hydrogen embrittlement for conventional duplex stainless steel and super duplex stainless steel was investigated.

2. Experimental

The base metals used in this investigation are 329J1, SAF2205 and SAF2507 duplex stainless steels. The samples were heated in the vacuum furnace at 923K-1223K for various times, and then water quenched.

Microstructure observation was carried out using electrolytic etching in 10kmol/m^3 KOH solution.

The etching technique colored sigma phase brown, colored ferrite blue and colored austenite white (in case of monochrome photography, the etching technique colored sigma phase black, colored ferrite gray and colored austenite white).

† Received on November 7, 2005

* Designated Professor

Transactions of JWRI is published by Joining and Welding Research Institute, Osaka University, Ibaraki, Osaka 567-0047, Japan

The area fraction of the sigma phase was measured by image processing on the basis of 30 fields of the optical micrographs at 500 magnifications in every sample.

TEM observation with an accelerating voltage of 200kV and X-ray diffraction analysis were used for observation and determination of sigma phase. Thin foil samples for TEM were prepared electrochemically using 10% perchloric acid in methanol.

Thin foils for transmission electron microscopy were prepared from 0.25 mm thick discs sliced from the plate. The discs were thinned to 0.05 mm by abrasion on SiC papers and twin-jet electro-polished in the solution below the temperatures of 243K.

An automatic reconstruction system for fractographic analysis was developed in this study[9]. The stereo images were obtained by making SEM images of the specimen tilted at two different angles to each other. 4º and 8º were adapted as the tilting angle between two images in the present study. The micrographs obtained were digitized using an image scanner with 256 gray levels.

The scanning resolution of digital images used was mainly 600dpi. After that the parallax between two images was measured by searching the corresponding points using an area-based matching algorithm. Cross-correlation was used for the evaluation. The elevation of the corresponding points can be computed. From the elevation data obtained, 3-D reconstruction images were displayed on a monitor via Open GL, the library for two-dimensional and three–dimensional computer programming. These programs were developed on “Microsoft Visual C++ 6.0” and designed to run under the Microsoft Windows platform of a PC .

3. Results and Discussion

3.1 Sigma phase and corrosion

Figure 1 shows transmission electron micrographs of type 329J1 duplex stainless steel, which was heated at 923K for 72ks. Darkened sigma phase are observed around the austenite phase as shown in Fig.1-(a). For more detailed observation as shown in Fig.1-(b), secondary austenite (named γ* phase) appeared between the primary austenite phase and the sigma phase.

The secondary austenite was more thinned than the primary austenite after the electrical thinning treatment. This suggests that the chemical composition of the secondary austenite is different from that of the primary austenite phase. Chromium and molybdenum contents in the secondary austenite seem to be less than those of the primary austenite[2].

$M_{23}C_6$ also precipitated between secondary austenite and primary austenite. Precipitation processes indicated that the precipitation of $M_{23}C_6$ occurred first, the secondary austenite formed next and then the precipitation of sigma phase occurred [11)-13)]. Though the orientation relationship between sigma phase and adjacent austenite phase is not as characteristic as

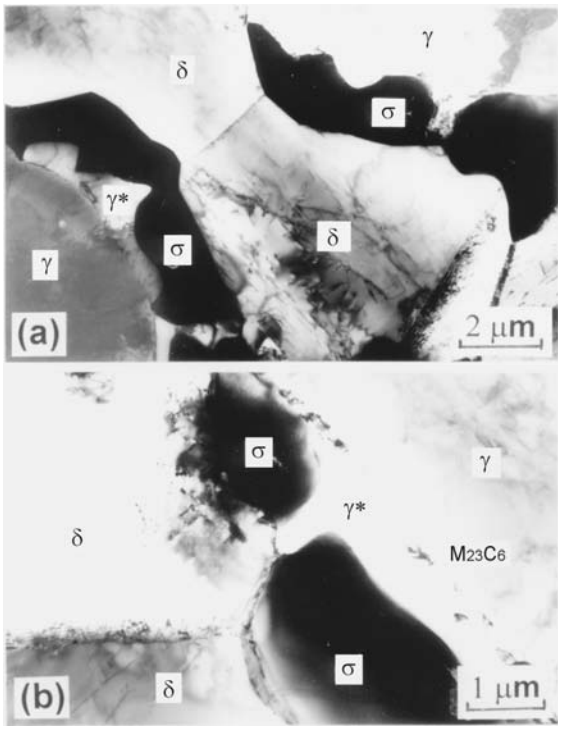

Fig.1 Transmission electron micrographs of type 329J1 steel heated at 923K for 72kS.

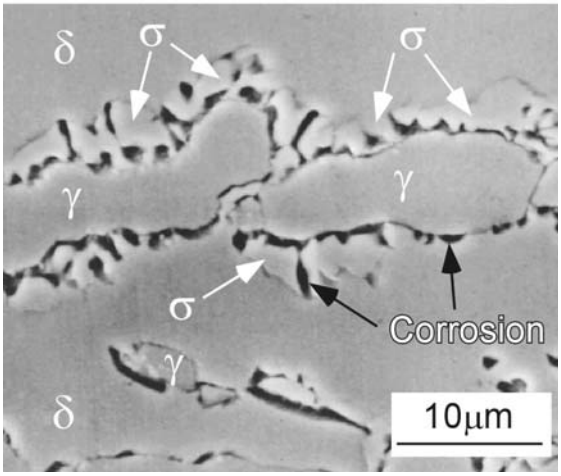

Fig.2 Surface appearance after Strauss test of type 329J1 steel heated at 923K for 72ks.

expected and deviates from the Nenno orientation relationship, a rational orientation relationship could be found between sigma precipitate and parent ferrite. During the growth of sigma phase at high temperature, the ferrite/sigma interface would become non-coherent and the morphology of sigma phase tends to be irregular shaped [2].

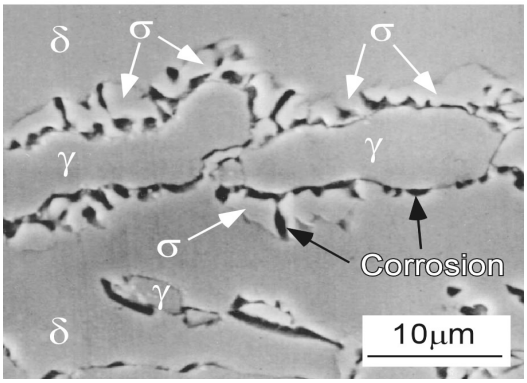

Fig.3 Microstructure of SAF2205 steel heated at 1223K for 7.2ks.

The fine secondary austenite (γ*) formation could be observed in the ferrite matrix. The secondary austenite formation was induced because precipitation of induced sigma phase depletes the adjoining ferrite matrix in chromium and molybdenum and enriches it in nickel and nitrogen.

The secondary austenite (γ*) enriches the adjoining ferrite matrix in chromium, molybdenum, which promotes the precipitation of sigma phase. As a result, it was assumed that the precipitation of sigma phase was accelerated more rapidly.

Figure 2 indicates a scanning electron micrograph of the surface appearance after the Strauss test for a type 329J1 specimen heated at 923K for 72ks. Black regions are localized corrosion areas. The corrosion preferentially initiated at the secondary austenite(γ*) between σ phase and γ phase. The secondary austenite, formed during the σ phase transformation (δ -- γ* + σ), is the phase that is primarily attacked by localized corrosion. In case of the Strauss test, the depleted zones below 13%Cr were preferentially corroded[14].

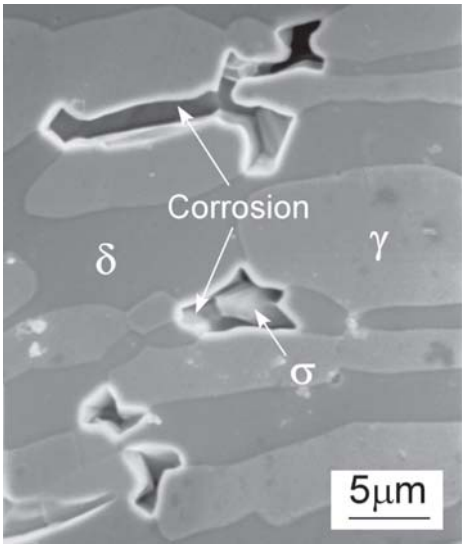

Fig.4 Corrosion appearance of SAF2205 steel heated at 1223K for 7.2ks.

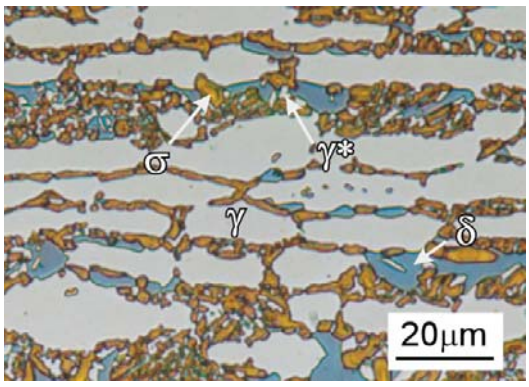

Fig.5 Microstructure of SAF2507 super duplex Stainless steel heated at 1223K for 7.2ks.

Figure 3 shows the microstructure of SAF2205 duplex stainless steel heated at 1223K for 7.2ks. The microstructure was revealed by electrical etching in KOH solution. The blue region is δ ferrite phase, white region is austenite(γ). The σ phase precipitated at δ/γ interface and grew up to the δ ferrite. The σ phases are observed as the block type and are of large size, between 2 μm to 5μm.

Figure 4 shows a scanning electron micrograph of the corrosion appearance of SAF2205 duplex stainless steel heated at 1223K for 7.2ks. The corrosion test was carried out by 10% oxalic acid test (ASTM A262A) and followed by etching in KOH solution. Localized corrosion occurred at the interface between δ phase and γ phases.

The initiation of localized corrosion took place around the σ phase due to depletion of Cr and Mo while the σ phase itself appears to be unaffected. Corrosion hardly occurred at the δ phase and γ phase interface. Wilms et al also reported that corrosion occurred around the σ phase, because the σ phase is rich in chromium and

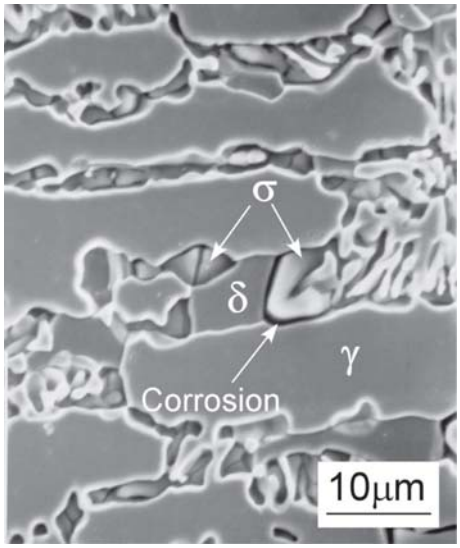

Fig.6 Corrosion appearance of SAF2507 steel heated at 1223K for 7.2ks.

molybdenum[19].

During the growth of the σ phase, these elements diffuse from the surrounding ferrite matrix to the σ phase.The change in the composition leads to the transformation of this region to austenite phase, referred to as γ*. At longer heating time, all the δ phase can be transformed to σ phase and secondary austenite (γ*).

Figure 5 shows the microstructure of SAF2507 super duplex stainless steel heated at 1223K for 7.2ks. Brown σ phases are precipitated at γ phase and δ phase. Small sizes of secondary austenite (γ*) are also observed. The precipitation particles are smaller than those in SAF2205 shown in Fig.3. The area fraction of sigma phase was measured. The results showed that the sigma phase amounted to 27% for the SAF2507 specimen and 12% for the SAF2205 specimen[10]. The σ phase precipitation in the SAF2507 specimen was much more than that in the SAF2205 specimen.

Figure 6 shows a scanning electron micrograph of the corrosion appearance of SAF2507 super duplex stainless steel heated at 1223K for 7.2ks. The corrosion test was carried out with the 10% oxalic acid test (ASTM A262A) and follwed by etching in KOH solution. Localized corrosion occurred around the σ phase. The Cr concentration in the area around the σ phase was less than that of the ferrite and that of austenite. Corrosion hardly occurred at the δ phase.

3.2 Sigma phase and hydrogen embrittlement

Figure 7 shows the relation between notch tensile strength and heating time at 1223K for SAF2205 duplex stainless steel. In the case of hydrogen free specimens, the notch tensile strength was 1170Mpa. The notch tensile strength decreased with increasing heating time. The area fraction of sigma phase was also measured. The σ phase increased with increasing heating time. In the case of a heating time of 600s, the area fraction of σ phase was 2%.

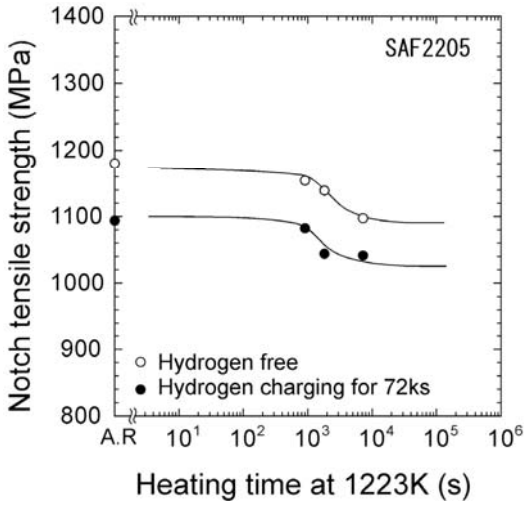

Fig.7 Relation between notch tensile strength and heating time at 1223K for SAF2205 duplex stainless steel.

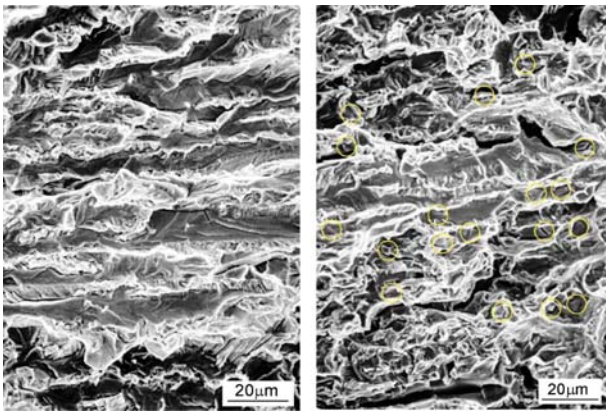

(a) Without heating (b) Heating at 1223K

Fig.8. Fracture morphology of hydrogn embrittlement for SAF2205 duplex stainless steel.

In case of 7.2ks, σ phase of 12% precipitated. Consequently, σ phase affected the lowering of notch tensile strength. After hydrogen charging, the notch tensile strength drastically decreased with increasing σ phase precipitation. A reduction from 1170MPa to 1090MPa was observed. The difference of strength between hydrogen free specimens and hydrogen charged specimens was almost the same independent of σ phase precipitation. This means that small amounts of σ phase up to 12% hardly affect hydrogen enbrittlement.

Figure 8 shows the fracture morphology of hydrogn embrittlement for SAF2205 duplex stainless steel. Fig.8-(a) shows the fracture morphology of the hydrogen embrittlement without heating. Transgranular quasi-cleavage fracture, particularly in the ferrite phase, was the predominant fracture mode[16].

The quasicleavage of the ferrite phase resulted in a

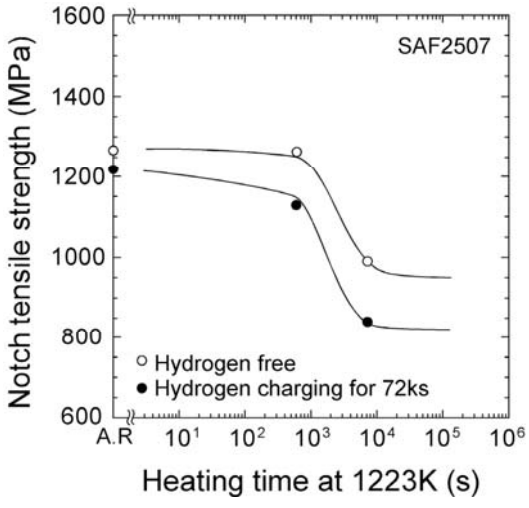

Fig.9 Relation between notch tensile strength and heating time at 1223K for SAF2507 steel.

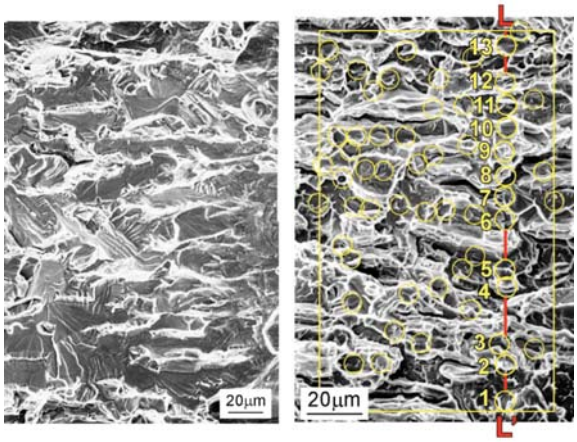

(a) Without heating (b) Heating at 1223K

Fig.10 Fracture morphology by hydrogen embrittlement for SAF2507 super duplex stainless steel.

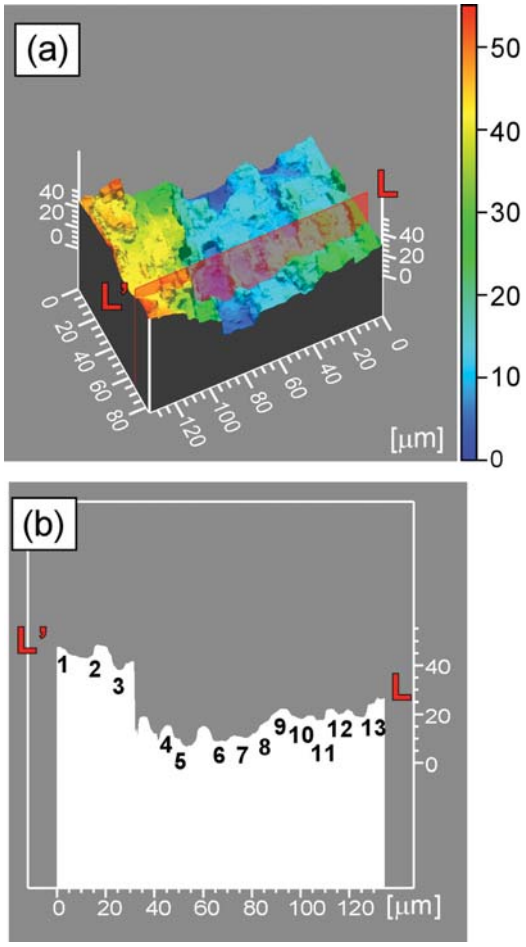

Fig.11 3-D reconstruction image (a) and 2-D image(b) for fracture morphology of hydrogen embrittlement for SAF2507 super duplex stainless steel.

large brittle facets, while the smaller cleavage facets in the austenite were associated with some plastic deformation. This may be partly a result of the higher susceptibility of the ferrite to hydrogen embrittlement owing to the high hydrogen diffusivity in ferrite (10^{-12} m^2s^{-1}) compared with that in austenite (10^{-16} m^2s^{-1})[17)-21)]. Quasicleavage fracture associated with plastic deformation in the austenite phase and faceted cleavage fracture in the ferrite phase were observed.

Fig.8-(b) indicates the fracture morphology of SAF2205 duplex stainless steel heated at 1223K for 7.2ks. The fracture morphology indicates a lot of elongated small size facets.

A lot of sigma phase was observed on the fracture surface as shown in the yellow open circle. The facet size is much smaller than that of the no-sigma specimen shown in Fig.8-(a). The amount of σ phase was 12% in microstructure. The fracture morphology of the sigma-hydrogen interaction shown in Fig,9-(b) is different to the normal hydrogen embrittlement specimen shown in Fig.8-(a)

Figure.9 indicates the relation between notch tensile strength and heating time at 1223K for SAF2507 super duplex stainless steel. The notch tensile strength of hydrogen free specimen was 1250MPa. After hydrogen charging, the strength was 1220MPa. The susceptibility to hydrogen of SAF2507 steel was lower than that of SAF2205 steel. However, the precipitation of sigma phase of SAF2507 steel was much more and much faster than that of SAF2250 steel[10)].

Sigma phase was 2% and 27% for the heating time 600s and 7.2ks respectively. After hydrogen charging, the notch tensile strength was drastically lowered with increasing σ phase. The σ phase precipitation affected notch tensile strength, and caused more hydrogen embrittlement for the SAF2507 super duplex stainless steel.

Figure 10 shows the fracture morphology of hydrogen embrittlement for SAF2507 super duplex stainless steel. Fig.10-(a) indicates the fracture morphology of hydrogen embrittlement without σ phase precipitation. Many cleavage fracture facets are observed in the ferrite matrix. Austenite phases occurred tear ridges by the plastic deformation. Fig.10-(b) indicates the fracture morphology of hydrogen embrittlement for the specimen in which σ phase precipitated. A lot of σ phase is observed on the fracture surface as shown in yellow open circles.

This means that the fracture propagated at the interface between σ phase and ferrite matrix. The fracture facet size of the sample was much smaller than that without σ phase specimen as shown in Fig.10-(a).

The region around σ phase is lower in Cr concentration. The strength of the Cr depleted zone seems to be lower than that of ferrite matrix. The plastic deformation concentrated in the Cr depleted zone[19)-22)], and the larger plastic deformation occurred in the depleted zone. Then hydrogen diffused there and the crack initiated at a lower tensile stress.It is considerd that the morphology of σ phase particle left on the fracture surface were observed. According to L-L' line, 13 sigma

particles are observed in the yellow open circles as the evidence.

Figure 11-(a) shows a 3-D reconstruction image of the fracture surface shown in Fig.11-(b). Many small mountains and valleys corresponded to each austenite morphology in the ferrite matrix. **Figure.11-(b)** shows a 2-D image of the L-L' section line. There are many small mountains and valleys. The digit number is identified to that shown in Fig.10-(b). Sigma phase was related to the fracture morphology of the super duplex stainless steel. The unit facet size is much smaller than that without sigma phase. The sigma phase precipitated around the austenite. Consequently, the fracture morphology of hydrogen embrittlement is related to the morphology of austenite, because of the sigma phase precipitated around the austenite phase.

4. Conclusions

The role of sigma phase on corrosion and hydrogen embrittlement for type 329J1, SAF2205 and SAF2507 duplex stainless steels was investigated by using corrosion test, transmission electron microscopy and 3-D fractography.

(1) Precipitation processes indicated that the precipitation of $M_{23}C_6$ occurred first, the secondary austenite formed next and then the precipitation of sigma phase occurred . The corrosion preferentially initiated at the secondary austenite(γ*) between sigma phase and γ phase. Chromium and molybdenum in the secondary austenite was less than that in the primary austenite.

(2) The sigma phase precipitation in the SAF2507 specimen was much greater than that in the SAF2205 specimen. The initiation of localized corrosion took place around the sigma phase due to the depletion of Cr and Mo while the sigma phase itself appears to be unaffected.

(3) The sigma phase precipitation affected the notch tensile strength, and hydrogen embrittlement of SAF2507 steel occurred more than that of SAF2205 steel. Fracture morphology of the hydrogen embrittlement was related to the morphology of austenite with sigma phase. The unit facet size was much smaller than that without sigma phase.

References

1) J.O.Nilsson, Mater.Sci.and Tech., **8**, 685 (1992).
2) J.O.Nilsson and A.Wilson, Mater. Sci. and Tech. **9** , 545 (1993).
3) G.Herbsleb, Werkst. Korros., **33** (1982).
4) T.J.Glover, Anti-Corrosion Methods Mater., **3,** 29 (1982).
5) T.Kuroda and F.Matsuda, Trans. JWRI **23-**4, 205 (1994).
6) T.Kuroda and F.Matsuda, Proc. 4th International Conf. Duplex '94, Glasgow, Scotland,(1994).
7) J.Charles, Proc. Conf. 'Duplex stainless steels'91', 3, Les Ulis, France, Les Editions de Physique. (1991).
8) T.Kuroda,Y.Kikuchi., Proc.Int.Conf. Joining of Materials (JOM8), Helsingor, Denmark, p376-381 (1997).
9) T.Kuroda, K.Ikeuchi and K.Nakade, J. Soc. Mat. Sci., Japan, **50-**11, 1170 (2001).
10) T.Kuroda, K.Nakade K.Ikeuchi, Welding in the World, **44,** p17-22, (2000)
11) D.J.Kotecki, Weld.J., 431s-441s (1989).
12) J.O.Nilsson., P.Jonsson., A.Wilson, Proc.4 th International Conf. Duplex'94, Glasgow Scotland, (1994).
13) T.Huhtala, J.O.Nilsson, A.Wilson ,P. Jonsson., Proc. 4th International Conf. Duplex '94, Glasgow, Scotland,(1994).
14) T. Kuroda and C.D Lundin., J. Soc. Mat. Sci., Japan, **73-**.488, 562-566 (1994).
15) F. Elshawesh and J.C. Scully, British Corrosion J. **33-**1 49-52（1998）.
16) W. Zheng and D. Hardie, Corrosion, **47-**10, 792-799 (1991).
17) J.W. Hsu, S.Y. Tsai and H.C. Shih, Corrosion **58-**10, 858-862 (2002).
18) F. Elshawesh, N. Elahresh, and A. Elhoud, BritishCorrosion j.**33-**4, 285-287 (1998).
19) M.E.Wilms, V.J.Gadgil, J.M.Krougman and F.P.Ijsseling, Corrosion Science, **39-**5, 871-881 (1994).
20) K. Ravindranath and S.N. Malhotra, Corrosion Science, **37-**1, 121-132, (1995).
21) Zheng and D. Hardie, Corrosion Science, **32-**1, 23-36,(1991).
22) R.A.Walker, Mater.Sci.and Tech., **4,** 78-84 (1988).